JOURNAL OF MATERIALS SCIENCE 20 (1985) 1383–1391

Influence of alloying elements silicon and tungsten upon the formation of chromium depleted zone in as-cast refractory steels

L. M. GRIBAUDO*, M. DURAND-CHARRE, S. HAMAR-THIBAULT
Institut National Polytechnique de Grenoble, LTPCM-ENSEEG, BP 75, 38402 Saint Martin d'Hères, France

Annealing of as-cast, high carbon, refractory alloys induces the formation of chromium-depleted zones in the austenite near the carbide–austenite interface. This depletion is a consequence of the drag of solute caused by the coarsening of the carbides. Micro-analytical investigation has been carried out to illustrate the depletion profiles and to obtain a semi-quantitative analysis of the tiny secondary precipitates. The equipment used included an electron microprobe, a scanning transmission microscope equipped with energy dispersive X-ray spectrometer (STEM/EDX)VG501, a transmission electron microscope (JEM200CX), and a scanning electron microscope (JSM-35). Extrapolation of the depletion curve gives the solute content in austenite at the interface. The values were correlated with the available thermodynamic data.

1. Introduction

The development of chromium-depleted zones surrounding the chromium carbides is often invoked to explain the good corrosion resistance of stainless steels. This chromium depletion of the matrix occurs as a consequence of carbide formation. In 1933 Bain *et al.* [1] proposed a model which assumes that when the chromium content decreases in the depleted zone below a critical value, this zone will lose its corrosion resistance. An electrochemical interpretation was given by Stickler and Vinkier [2]. Stawstrom and Hillert [3] established a model involving a diffusion controlled mechanism for the drag of solute. This model has been applied to low carbon austenitic stainless steels. These steels display $M_{23}C_6$ carbides as secondary precipitates located at the grain boundaries. Tedmon *et al.* [4] proposed a model fairly similar to the preceding one. Moreover, they assumed that the volume diffusion of chromium in the matrix could be ignored, the grain boundary diffusion being the main mechanism. This drag of solute does not occur only at grain boundaries but also in the vicinity of the solidification carbides in high carbon steels. In this case the formation of the depleted zone may occur at a higher temperature. Consequently, this zone is larger since its width depends on temperature allowing detection by microprobe investigations [5].

More recently micro-analytical methods have been available with sufficient spatial resolution to resolve such narrow regions. Lackey and Humphreys [6] and Thorvaldsson and Dunlop [7], studied chromium depletion profiles near the grain boundaries using scanning transmission electron microscopy with energy dispersive X-ray spectrometry (STEM/EDX). The latter authors have shown that the formation of chromium-depleted zones can occur at the grain boundaries of niobium and titanium stabilized stainless steels.

Our purpose was to investigate AISI 310 stainless steels containing additions of silicon and

Present address: INTEC, C.C. No. 91, Santa Fe, Argentina.

0022–2461/85 $03.00 + .12

TABLE I Composition of alloys (wt%), A1, A2, A3, A4 are modified alloys, R, T, V, are commercial alloys

Sample	C	Cr	Ni	Si	W	Mn	S	P
A1*	0.4	24.9	21.0					
A2*	0.4	23.6	19.6	2.0				
A3†	0.4	23.0	20.5		2.8			
A4†	0.4	22.9	20.5	2.8	1.0			
R†	0.4	24.7	19.7	1.0	2.8	0.9	0.01	0.01
T*	0.4	24.5	19.5	2.0	2.8	0.9	0.01	0.01
V*	0.5	24.5	24.5	1.9	1.8	1.9	0.01	0.02

*Eutectic carbides are M_7C_3.
†Eutectic carbides are $M_{23}C_6$.

tungsten. In a previous study [8] we established that these additions promote, in high carbon steels, the formation of either $M_{23}C_6$ or M_6C eutectic carbides. During the cooling process these carbides act as collectors for chromium in the supersaturated matrix. According to the temperature a thermodynamic equilibrium is established at the interface between carbide and matrix. Carbon is supposed to diffuse rapidly since its diffusion coefficient is several orders of magnitude higher than for other elements and its activity dictates the chromium level. At first, our aim was to determine if there was any substantial difference in the concentration profiles of each element in the vicinity of the carbides. We then tried to observe the evolution of secondary precipitates with ageing time.

2. Experimental techniques

The chemical composition of the alloys which have been studied is reported in Table I. Some of them: Al; A2; A3; A4, have been prepared in the laboratory with high purity metals. Others: R; T; V, are plain commercial steels. All the alloys have about the same carbon content which is 0.4 wt%. As a consequence of this high carbon content, the solidification finishes by forming an eutectic structure in the interdendritic groove. The eutectic carbides are of the M_7C_3 type for compositions A1, A2, T, and V, and of $M_{23}C_6$ type for compositions A3, A4, and R (Table II, [8]). Quenched-interrupted directional solidification (QIDS) has been performed on alloys R and V so as to obtain coarser and more characteristic structures. Other alloys have been solidified and cooled in differential thermal analysis apparatus at a controlled cooling rate of $300^\circ C\,h^{-1}$. Some of those samples have been heat-treated in a quartz, sealed tube at 750° C for different ageing times up to 1000 h.

The metallographic examination was carried out with an electron microprobe (MSE), a scanning transmission electron microscope equipped with an energy dispersive X-ray spectrometer (STEM/EDX) VG501, a transmission electron microscope (JEM 200 CX), and a scanning electron microscope (SEM, JSM-35). Analysis of the finest regions, such as secondary carbides, was performed on thin foils using STEM/EDX. Thin foils were prepared by electropolishing in a 700 ml ethyl alcohol, 100 ml glycerol and 200 ml acetic acid solution at 15° C under 10 V.

Concentration profiles of chromium within the matrix obtained by MSE are fairly coarse on a macroscopic scale. More accurate investigation was made on bulk samples with SEM/EDX. The specimens must be carefully prepared, that is polished with 1/4 μm diamond powder. Particular attention

TABLE II STEM/EDX analysis

Alloy	Adjacent Carbide	C_b	C_i	$\frac{C_b - C_i}{C_b}$	l(μm)
A (25–20)	M_7C_3	0.249	0.197	0.21	2.4
A (25–20 + Si)	M_7C_3	0.238	0.167	0.30	2.6
A (25–20 + W)	$M_{23}C_6$	0.230	0.147	0.36	2.5
A (25–20 + Si + W)	M_6C	0.231	0.166	0.28	2.3
	$M_{23}C_6$		0.148	0.36	
T (25–20 + Si + W)	M_6C enclosing M_7C_3	0.246	0.178	0.28	4.7
V (25–25 + Si + W) QIDS	M_7C_3	0.252	0.184	0.27	4.7
V (25–25 + Si + W) annealed 90 h at 750° C	M_7C_3	0.251	0.188	0.25	5.3

C_b, concentration of chromium in the bulk (atomic fraction).
C_i, extrapolated concentration of chromium at the interface (atomic fraction).
l, diffusion length.

was given to control the reproductibility of the experimental conditions. The values were obtained using the ZAF method (Z = atomic number, A = absorption, F = fluorescence). The nearest point we can most reliably analyse is at 900 nm from the interface. Assuming that equilibrium is reached at the interface, the development of the chromium profile is given by a solution of Fick's second law for diffusion:

$$C_z = C_i + (C_b - C_i) \operatorname{erf} Z/2(Dt)^{1/2} \quad (1)$$

where: C_i, C_z are chromium concentrations respectively at the interface and at a distance z from the interface; C_b is the chromium concentration in the bulk; D is the diffusion coefficient of chromium; and t is time.

The ultimate value at the interface is obtained by fitting the experimental curve with the preceding law. Profiles of concentration have been carried out on a still finer scale using STEM/EDX analysis on thin foils. The critical point is that this method would require a constant thickness of the foil. Relative proportions of the various elements are determined by the ratios of the corresponding areas on the energy spectrum.

3. Results concerning the chromium-depleted zone

The microstructure of a unidirectionally solidified rod of alloy V is illustrated in Fig. 1. We can distinguish two levels on the rod: level L represents the part which has been quenched just at the end of solidification; level M corresponds to a part which has been kept at high temperatures for 45 min. The microprobe solute profiles have been drawn at these two levels. At level L the profile reveals two kinds of peaks. The peaks, indicating a high chromium content and a low silicon content, correspond to the white phase on the micrograph which has been identified in a previous study [8] as M_7C_3 carbides. The peaks indicating simultaneously a high tungsten and silicon content, correspond to the black phase on the micrograph, identified as M_6C carbides. In addition, differences of solute content in the matrix are noticeable, they are due to segregation occurring during solidification. This segregation is rather severe for tungsten and silicon. At level M there occurs a chromium depletion adjacent to the M_7C_3 carbides (indicated by a couple of arrows), which is due to the diffusion controlled growth of carbides.

Fig. 2 presents the STEM/EDX chromium profiles in the vicinity of the M_7C_3 carbide interface for alloy V. The upper curve corresponds to the alloy slowly cooled during unidirectional solidification. The bottom curve corresponds to the same alloy aged for 90 h at 750° C. In this case secondary precipitates have been observed on the electron transmission micrographs as little as 5 μm from the interface. As a consequence, an increase of chromium is detected very locally but cannot be taken into account as a measure of the matrix content. However, a tendency can be noted: long time ageing promotes a slight increase of chromium concentration at the interface.

Table II summarizes all the results concerning the profiles. For each composition we have indicated the nature of the solidification carbides in the neighbourhood of which the profile was determined. C_i and C_b represent the concentrations respectively at the interface and in the matrix analysed in the same conditions. Compared to the initial compositions (Table I), it appears that all the values are slightly overestimated on account of the analysis method. ΔC represents the gap caused by depletion, normalized in relation to the bulk content. The diffusion distance, L, is determined by drawing a tangent at the interface on the depletion curve. This value, which is proportional to $(Dt)^{1/2}$, gives an estimate of the diffusion time for a constant temperature. The level of chromium content C_i is different for each alloy, being lower when the alloy contains either silicon, tungsten or both. The difference between the bulk composition in the matrix and the concentration at the interface varies similarly: it increases significantly with the addition of alloying elements.

Fig. 3 shows the micrograph of a thin foil of Alloy A3 and the corresponding analysis with STEM/EDX. The gap of depletion as previously defined $(C_b - C_i)/C_b$ is 0.35, which is in perfect agreement with the other value reported in Table II for the same alloy.

Complex M_6C carbides may occur at the end of the solidification in the inter-dendritic groove in the last liquid enriched in chromium, silicon and tungsten on account of solidification segregation. Alloy T, which has the highest content in alloying elements, exhibits such a microstructure (Fig. 4). Back-scattered electron and X-ray micrographs show that all the M_7C_3 carbides are enclosed in a M_6C layer. In this case local equilibrium adjacent to the M_7C_3 carbides is to be compared to the

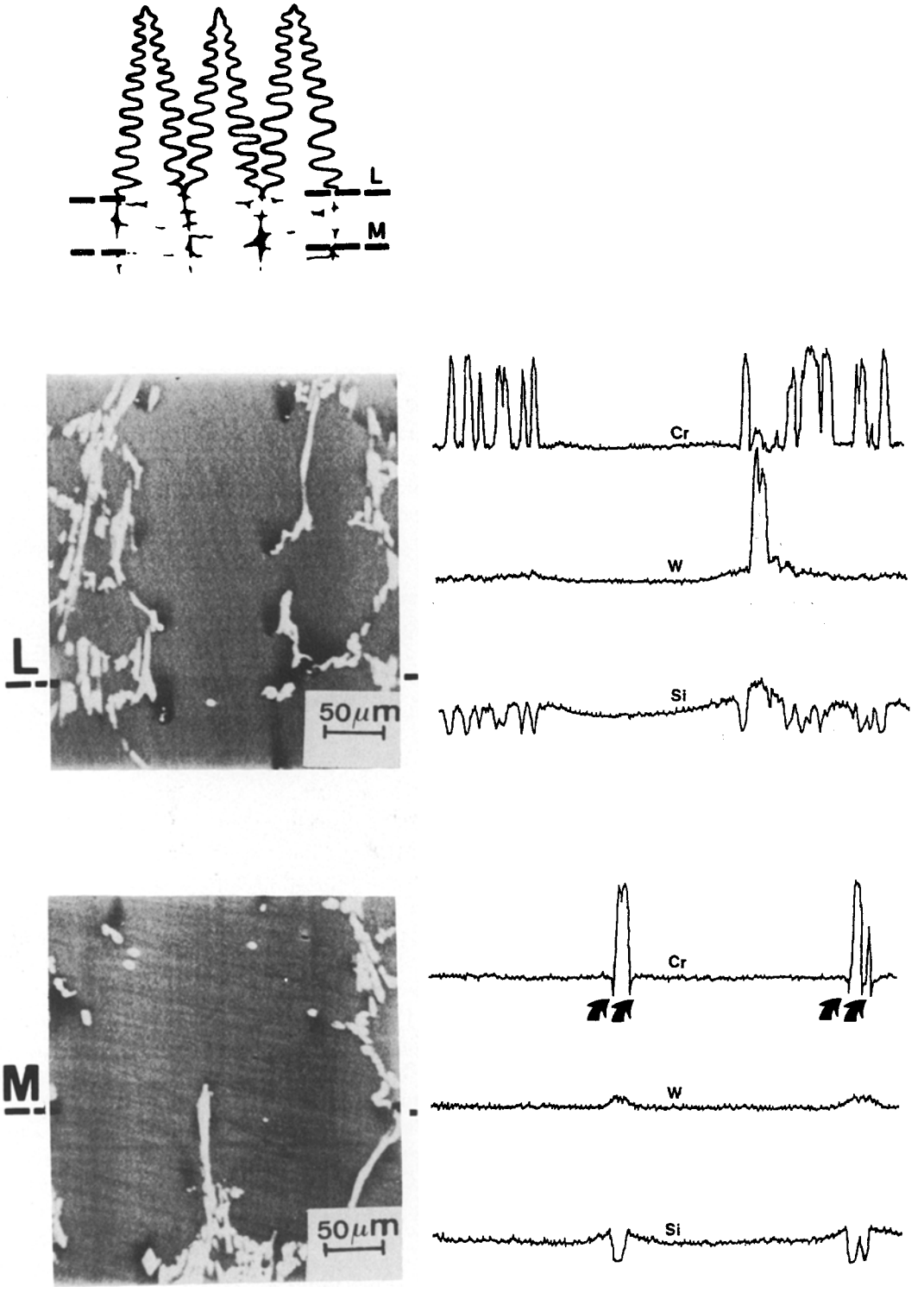

Figure 1 Microstructures of a rod unidirectionally solidified then quenched, and the corresponding microprobe solute profiles at levels L and M. The arrows indicate the chromium depleted zone.

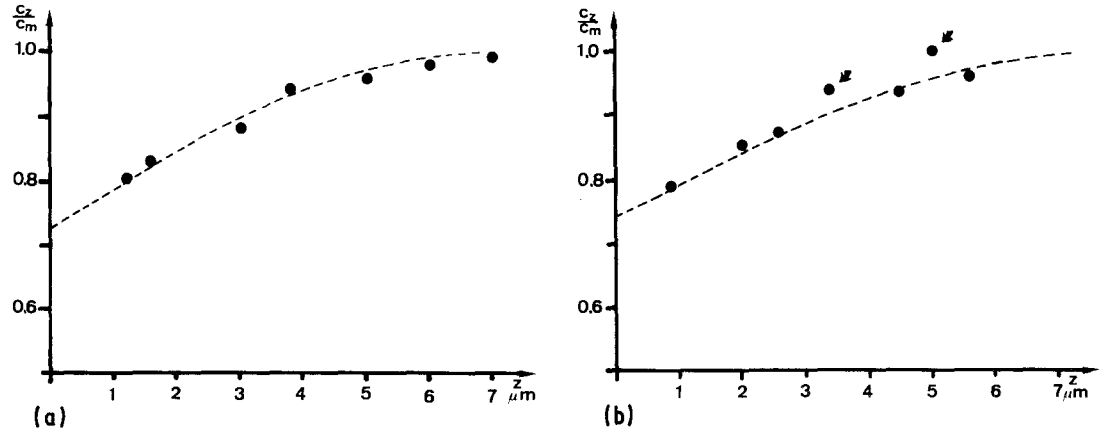

Figure 2 STEM/EDX analysis of chromium concentration in the vicinity of M_7C_3 eutectic carbides for alloy V. (a) At level M on Fig. 1 (b) After 90 h annealing at 750° C.

equilibrium near M_6C in the alloy A4, for which the values are reported in Table II.

4. Results concerning secondary precipitation

The alloys R and V have been annealed for 1000 h at 750° C. Fig. 5 illustrates their microstructures after ageing. Alloy V exhibits coarse $M_{23}C_6$ precipitates, while alloy R contains smaller, coherent $M_{23}C_6$ precipitates. This precipitation may be detected on the microprobe profiles since they appear jagged. All the precipitates have been identified as $M_{23}C_6$. The experimental observations made by TEM and STEM/EDX are reported in Table III.

Fig. 6 corresponds to the examination of a thin foil by STEM/EDX for alloy V. Three kinds of precipitates are shown on the micrograph: large $M_{23}C_6$ carbides (about 2 μm) with a high chromium ratio; smaller coherent $M_{23}C_6$ precipitates (about 0.3 μm) whose chromium ratio ranges between 0.5 and 0.8; plate-shaped precipitates with a very high tungsten content. One of these latter precipitates has been extracted in order to carry out a more accurate identification. Note that the tungsten content is too high to correspond to a M_6C carbide. The diffraction pattern shows that it can be indexed as Laves phases of $(Cr, Fe, Ni)_2W$ type with a hexagonal structure (a = 0.476 nm, c = 0.77 nm) (Fig. 7). These lattice parameters are very close to the ones of Fe_2W (a = 0.473 nm c = 0.70 nm). In addition to the analysis of the carbides we tried to establish the chromium content profiles near the secondary carbides. Close to the largest chromium rich carbides the profile exhibits the usual depleted zone. In contrast, near the smallest carbide there is an enriched zone as if the carbide was dissolving and losing its chromium (Fig. 8).

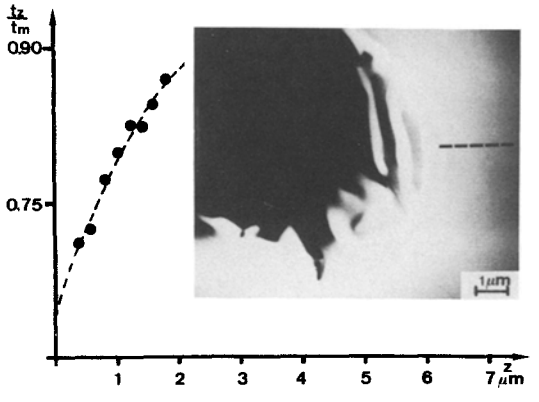

Figure 3 STEM/EDX micrograph and analysis in the vicinity of $M_{23}C_6$ eutectic carbide in alloy A.

TABLE III Recapitulation of results concerning secondary precipitation

	Alloy R	Alloy V
Solidification carbides	$M_{23}C_6$ – M_6C	M_7C_3 – M_6C
Secondary precipitates	$M_{23}C_6$ $t \simeq 0.8$ $\phi = 0.5\,\mu m$	$M_{23}C_6$ $0.5 < t < 0.8$ $\phi = 0.3\,\mu m$ $M_{23}C_6$ $t \simeq 0.8$ $\phi = 2\,\mu m$ Laves phase $\phi \simeq 0.1\,\mu m$

t indicates the chromium content and ϕ the mean diameter of $M_{23}C_6$ precipitates.

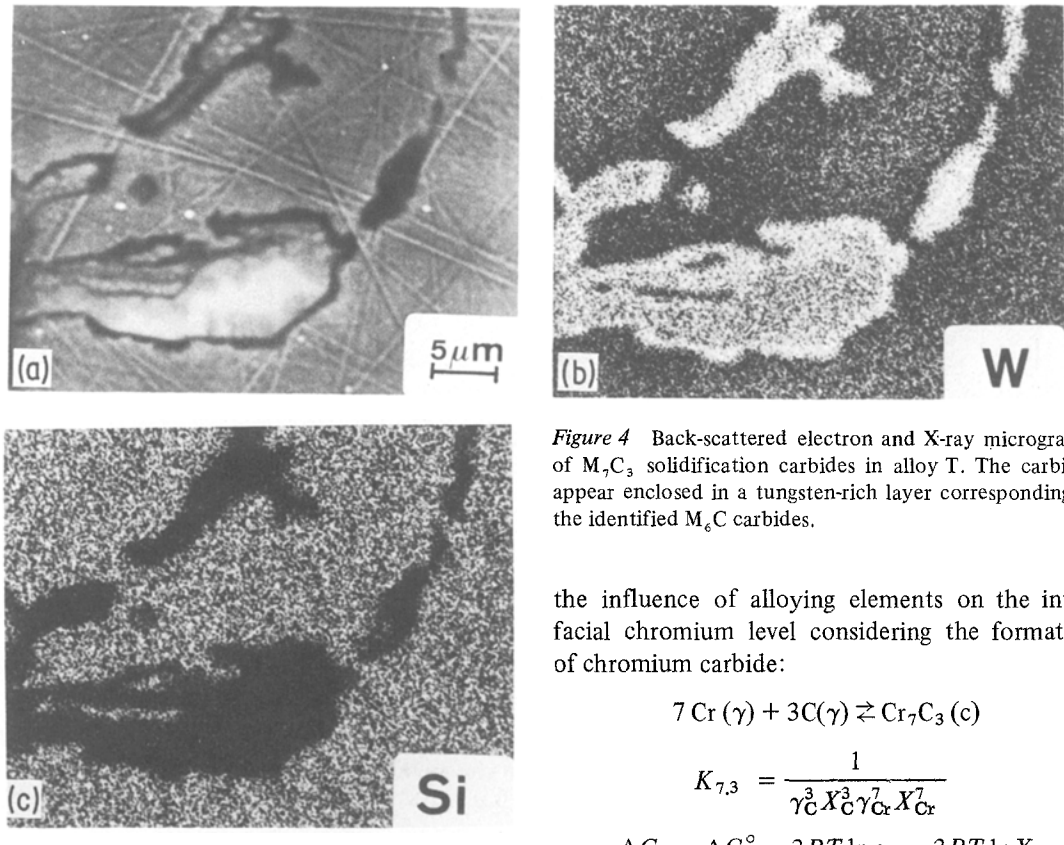

Figure 4 Back-scattered electron and X-ray micrographs of M_7C_3 solidification carbides in alloy T. The carbides appear enclosed in a tungsten-rich layer corresponding to the identified M_6C carbides.

5. Discussion

It is a diffusional mechanism that controls the whole precipitation reaction. The model proposed by Stawstrom and Hillert [3] involves several stages which are: an early stage during which the depleted zone occurs and enlarges; then a stage of self-healing. On prolonged annealing, as precipitation of $M_{23}C_6$ carbides gradually increases, the carbon activity decreases. The equilibrium changes and the chromium content will thus set itself higher. The situation at the $M_{23}C_6$ carbide–austenite interface may be described by the tie-lines in the phase diagram. Durand-Charre *et al.* [5] proposed a similar explanation for alloys containing eutectic carbides M_7C_3. In this case the carbon activity which defines the interface equilibrium is maintained at a level compatible with the equilibrium between M_7C_3, $M_{23}C_6$ and austenite.

After a very long ageing time M_7C_3 disappears and the chromium content at the interface rises in a self-healing process. Of course for more complex alloys, containing more than three elements, a discussion based on a ternary phase diagram would not be accurate any more. However, we can discuss the influence of alloying elements on the interfacial chromium level considering the formation of chromium carbide:

$$7\,Cr\,(\gamma) + 3C(\gamma) \rightleftarrows Cr_7C_3\,(c)$$

$$K_{7.3} = \frac{1}{\gamma_C^3 X_C^3 \gamma_{Cr}^7 X_{Cr}^7} \tag{2}$$

$$\Delta G = \Delta G^\circ_{7.3} - 3RT \ln \gamma_c - 3RT \ln X_c - 7RT \ln \gamma_{Cr} - 7RT \ln X_{Cr} \tag{3}$$

where: γ is the activity coefficient; X is molar fraction; and $\Delta G = 0$ for equilibrium. Some assumptions have been made: as previously mentioned γ_c is a constant on account of high carbon diffusivity. Moreover, γ_{Cr} is almost independent of the composition for a constant content of chromium. The relation becomes:

$$\Delta G^\circ_{7.3} - 3RT \ln \gamma_C - 7RT \ln X_{Cr} - \text{constant} = 0$$

$$d(\Delta G^\circ_{7.3}/RT) + 3d\ln \gamma_C + 7d\ln X_{Cr} = 0 \tag{4}$$

As the silicon in M_7C_3 is very small, it can be neglected and $\Delta G_{7.3}$ remains unchanged. On the contrary silicon modifies the carbon activity coefficient. Scherbedisiskii [9] proposes a value for the Wagner coefficient:

$$\frac{\partial \ln \gamma_C}{\partial X_{Si}} = 5.4$$

Addition of 2 wt% silicon ($dx = 0.0383$) in a 25Cr20Ni alloy increases γ_C by an amount $d\ln\ \gamma_C = 0.207$. Consequently, the chromium

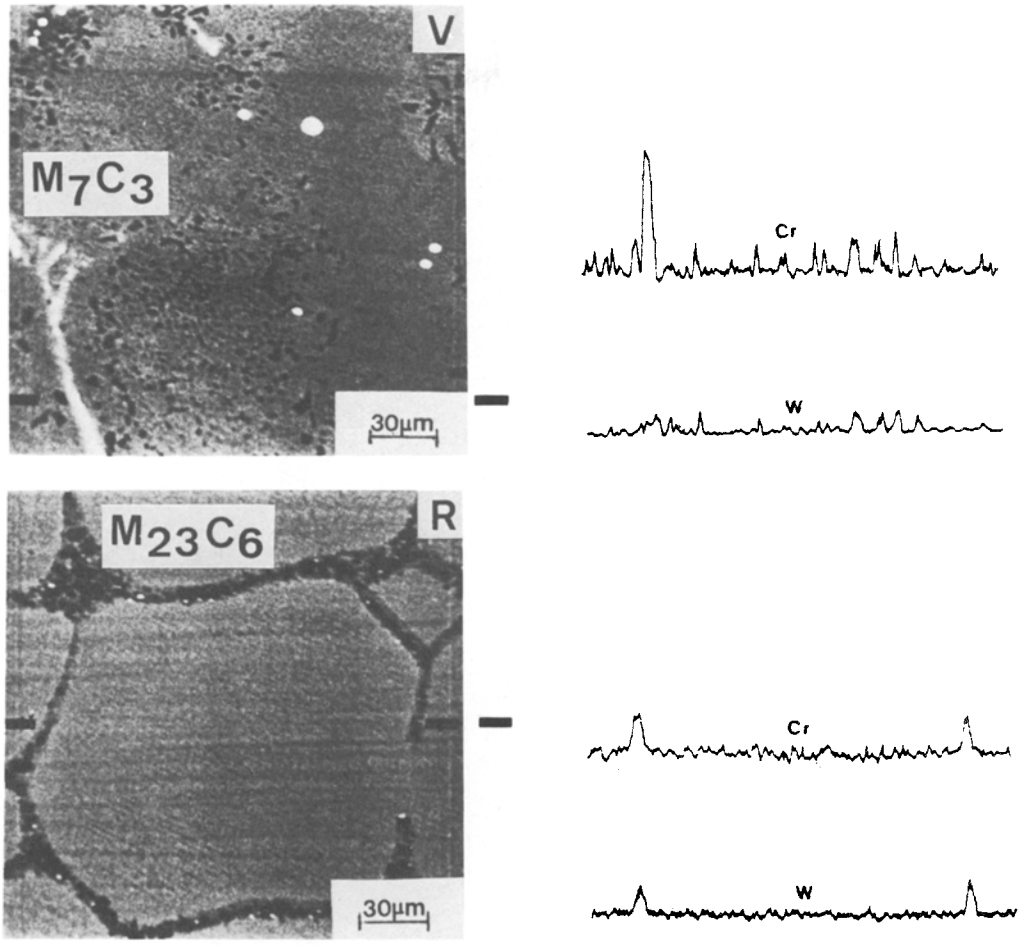

Figure 5 Back-scattered electron micrographs and microprobe analysis profiles for alloys V and R aged for 1000 h at 750° C.

equilibrium is lowered, $d\ln\gamma_{Cr} = -8.9 \times 10^{-2}$. The comparison of this latter value with the ΔC corresponding to alloys A1 and A2 (Table II) shows a good agreement between the thermodynamic calculations and the experimental values.

We attempted to explain in the same manner the influence of tungsten in austenite on the austenite–carbide equilibrium. In this case the thermodynamic calculations do not fit with experimental results. Wagner's interaction coefficient predicts an opposite effect. Moreover, as $M_{23}C_6$ contains tungsten, the thermodynamic value for $\Delta G_{23,6}$ is modified. Considering the respective approximate formulae for carbides ($Cr_{17}(Fe, Ni)_5W\ C_6$; $Cr_{6.1}\ Fe_{0.8}\ W_{0.1}\ C_3$) the tungsten amount cannot be neglected as it was for M_7C_3 [8]. The calculation of a new $\Delta G_{23,6}$ from an ideal model does not provide a good agreement. We would need more thermodynamic data to achieve a reliable prediction.

Hillert and Waldenstrom [10] determined thermodynamic equilibrium in the Fe–Cr–Ni–C–Mn system. A comparison may be made between the influence of manganese and tungsten; it is justified because in both cases Wagner's interaction coefficients are negative [10, 11] and the solute acts as a substitutional element within the carbide. Their finding was that manganese lowers the chromium content in austenite for a given carbon activity which is similar to our own experimental results.

Another result that we cannot explain is that the chromium depletion is not as severe in the vicinity of M_6C carbides as it is in the vicinity of the other carbides (Table II). This result is important considering that a higher chromium level

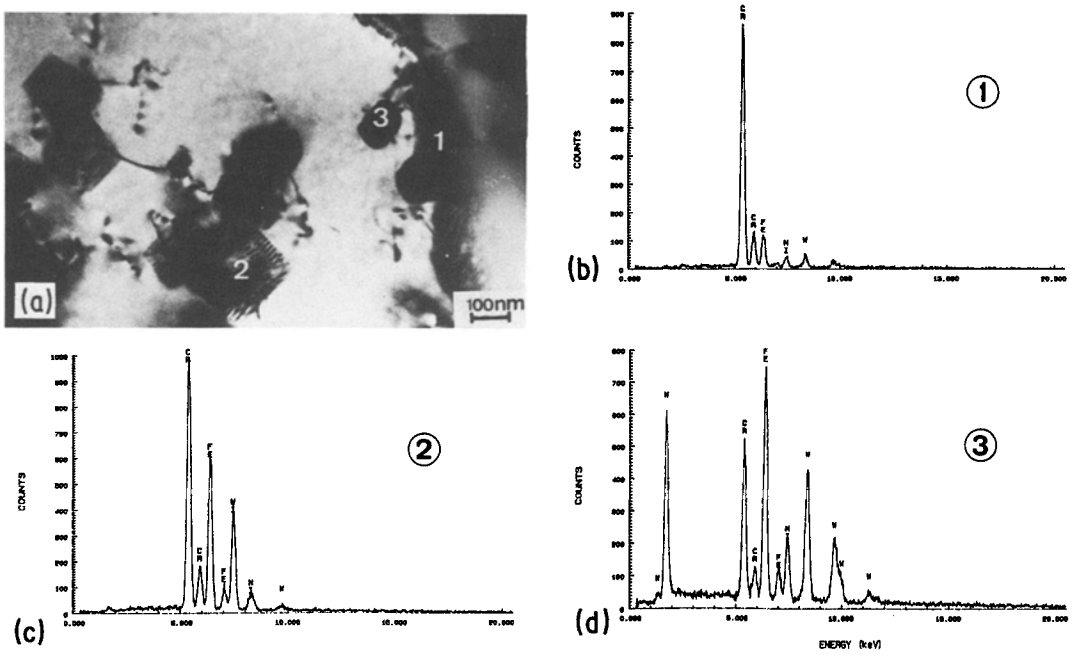

Figure 6 (a) STEM micrograph illustrating the different kinds of precipitates for alloy V aged for 1000 h at 750° C and the corresponding energy dispersion X-ray spectra for: (b) large secondary carbide, (c) small carbide, (d) Laves phase.

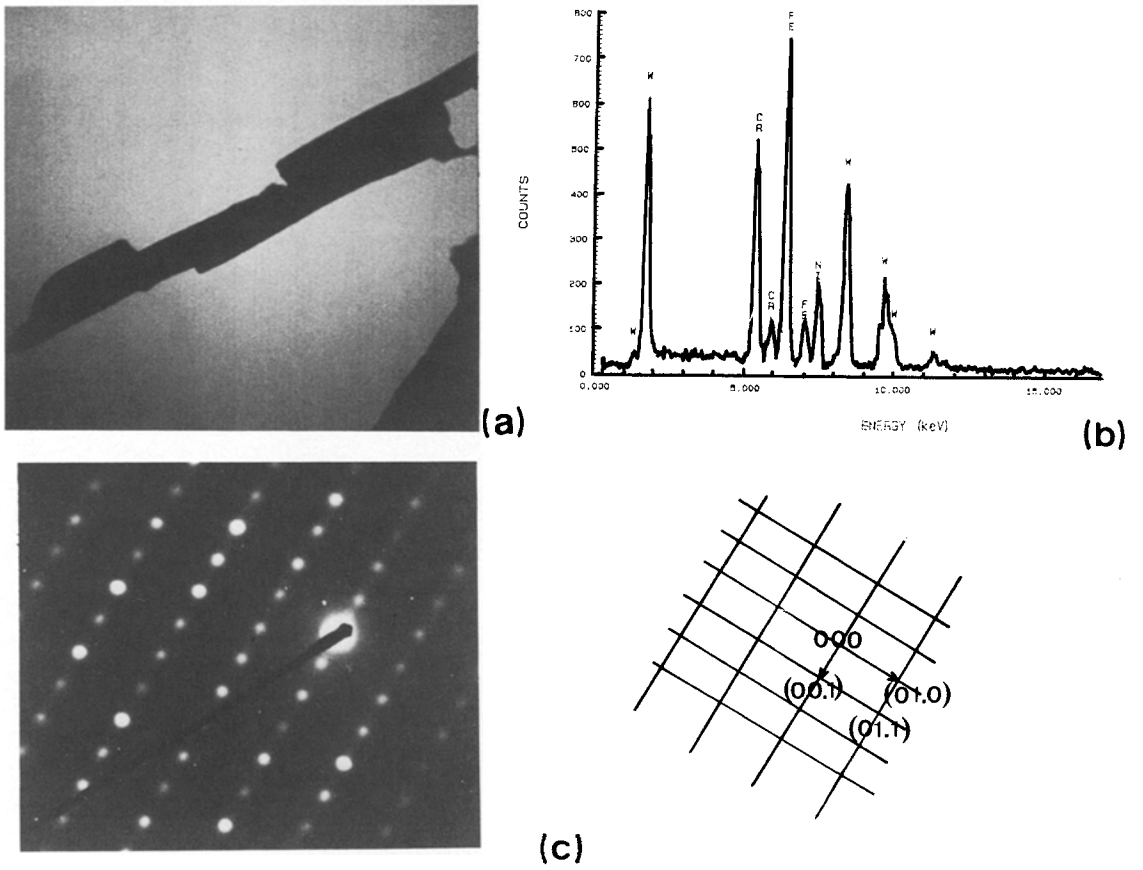

Figure 7 Identification of Laves phases in alloy V, (a) STEM micrograph, (b) energy dispersion X-ray spectra, (c) diffraction pattern and key diagram.

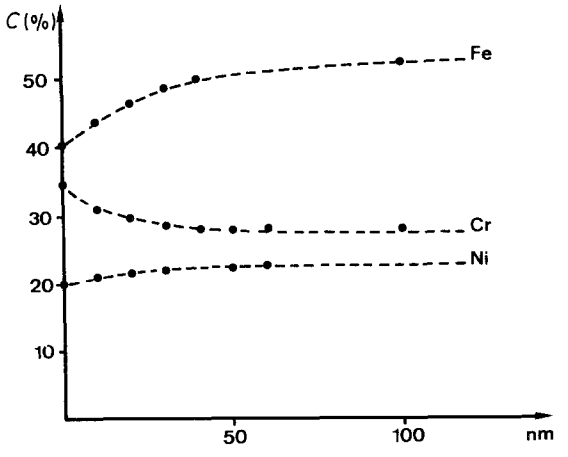

Figure 8 STEM/EDX analysis of solute concentration in the vicinity of small secondary $M_{23}C_6$ carbides.

involves a better resistance to localized corrosion [12]. Gribaudo and Rameau [13] have established an order of nobility for the matrix and the different carbides which predict whether localized corrosion occurs in the depleted zone or not.

It is only recently [14] that the evolution of the composition of secondary precipitates has been investigated. Boeuf *et al.* [15], and Thorvaldsson *et al.* [16] found an enrichment of chromium against iron when ageing time increases. After a long annealing time near 800° C, the more stable carbides are the chromium richer ones. Consequently the less chromium-rich carbides are unstable; they dissolve, providing carbon and chromium which facilitates the coarsening of the other carbides. This explanation fits with the two kinds of chromium profiles which have been found (Fig. 8).

6. Conclusion

The chromium depletion in the vicinity of the carbides is a consequence of the drag of solute occurring during the growth of carbides upon annealing. The chromium content in the austenite at the interface depends upon the thermodynamic equilibrium. By examination of chromium profiles we have shown that solute elements such as silicon and tungsten influence the equilibrium. They both lower the chromium content in the depleted zone.

The use of recent microanalytical methods enables us to give evidence of the evolution of secondary carbides. As the final equilibrium involves chromium-rich carbides, previously formed and less-rich secondary carbides dissolve while chromium-rich carbides coarsen.

References

1. E. C. BAIN, R. H. ABORN and J. J. RUTHERFORD, *Trans. Amer. Soc. Steel Inst.* **21** (1933) 481.
2. R. STICKLER and A. VINCKIER, *Corros. Sci.* **3** (1963) 1.
3. C. STAWSTROM and M. HILLERT, *JISI* **207** (1969) 77.
4. C. S. TEDMON, D. A. VERMILYEA and J. H. ROSOLOWSKI, *J. Electrochem. Soc.* **118** (1971) 192.
5. M. DURAND-CHARRE, B. CHOVELON, N. VALIGNAT and J. J. RAMEAU, *Mem. Sci. Rev. Met. Paris* **77** (1980) 717.
6. M. G. LACKEY and F. Y. HUMPHREYS, Proceedings of the 3rd International Conference on Hydrogen, Moran, 1980, (AIME, Philadelphia, 1981), 665.
7. J. THORVALDSSON and G. L. DUNLOP, *J. Mater. Sci.* **18** (1983) 793.
8. L. GRIBAUDO, F. DURAND and M. DURAND CHARRE, *Mem. Sci. Rev. Met. Paris* **80** (1983) 211.
9. G. V. SCHERBEDISISKII and V. I. SHAIDUVOV, *Zh. Fiz. Khim.* **42** (1968) 660.
10. M. HILLERT and M. WALDENSTROM, Mac Rapport 0102 (Mat. Center Royal Inst. Stockholm, 1976).
11. M. A. KRISHTAL and Y. I. DAVIDOV, *Izv. Chern. Met.* **9** (1965) 133.
12. D. SINIGAGLIA, P. FASSINA, D. WEGNER and G. RE, *Corrosion* **38** (1982) 95.
13. L. GRIBAUDO and J. J. RAMEAU, *Corros. Sci.* **4** (1984) 291.
14. J. PHILIBERT, G. HENRY, M. ROBERT and J. PLATEAU, *Mem. Sci. Rev. Met. Paris* **58** (1961) 557.
15. A. BOEUF, R. CACIUFFO, S. CRICO, R. REBONATO, F. RUSTICHELLI and J. P. MORLEVAT, *J. Mater. Sci. Lett.* **2** (1983) 49.
16. T. THORVALDSSON, H. RUBINSZTEIN DUNLOP, H. O. ANDREN and G. L. DUNLOP, Proceedings of the Conference on Quantitative Microanalysis with high Spatial Resolution, Manchester, 1981.

Received 5 December 1983
and accepted 4 June 1984